Kovove Mater. 57 2019 105–111
DOI: 10.4149/km_2019_1_105

Mechanical properties of aluminum foams ceramic coated through plasma electrolytic oxidation

F. Çavuşlu[1,2]*, K. Korkmaz[1], M. Usta[1,3]

[1]*Department of Materials Science and Engineering, Gebze Technical University, Gebze, Kocaeli 41400, Turkey*
[2]*Department of Materials Engineering, Adana Science and Technology University, Adana 01250, Turkey*
[3]*Materials Institute, Marmara Research Center, The Scientific and Technological Research Council of Turkey (TÜBİTAK), Gebze, Kocaeli 41470, Turkey*

Received 25 June 2018, received in revised form 9 October 2018, accepted 14 November 2018

Abstract

Plasma electrolytic oxidation (PEO) treatment is carried out to improve the mechanical properties of the open-cell aluminum foams. Two different pore densities of open-cell aluminum foams (20 PPI and 40 PPI) were treated in an alkaline solution with a low silicate concentration at different current densities and times. The microstructure and phase composition of samples were investigated by scanning electron microscope (SEM) and X-ray diffraction (XRD) respectively. The coating thickness of the struts was increased with the increasing of treatment time. Ceramic coatings were composed of corundum, gamma alumina, and mullite phases. It was found that the compressive properties of the pore density of 20 PPI composite foams were significantly improved by using PEO treatment.

K e y w o r d s: plasma electrolytic oxidation, aluminum foams, surface treatment, mechanical properties

1. Introduction

Metallic foams are lightweight materials increasingly used in structural and functional applications. A great deal of research has been carried on over the past decades. These foams have low strength, unlike its bulk counterparts. However, metallic foams exhibit high stiffness to weight ratio and can absorb large energy at a nearly constant stress level [1, 2]. Metallic foams made of aluminum and its alloys are widely used for their lightweight, low casting temperature, and high corrosion resistance [3].

Significant advances have been made to characterize and enhance the mechanical behavior of these emerging materials. The mechanical properties of foams were simulated concerning their cell structure. It has been suggested that open cell foams deformed by bending of the cell edges, while closed cell foams deformed by stretching of the cell faces in addition to bending of the cell edges [1].

Any attempts to improve the bending of the cell edges have been the main aim of the researchers. Dispersion strengthening by adding second phase particles [4] and coating the cell edges with stiffer and harder materials are the methods to accomplish the above attempts. The latter method includes electrodeposition [5–7], anodizing [8], and plasma electrolytic oxidation (PEO) [9–12] treatments in which aluminum foams are coated in an aqueous electrolytic solution.

PEO is a novel surface treatment process in which the conventional anodic oxidation process is carried out in alkaline solutions at high electrical voltages. PEO process transforms the surface of light metals such as Al, Mg, Ti, and Zr and their alloys into ceramic oxides. In this process, by the application of the voltage, the oxide of the metal starts to form on its surface. Above the breakdown voltage of this oxide film, micro-arc discharges are developed in the surface layer. Then, the plasma-enhanced chemical and electrochemical reactions occur through the discharge channels. The crystallization, sintering, formation, and transformation of ceramic oxide phases take place in these discharge channels. When the discharge channels are entirely filled with the ceramic oxides, they are exposed to rapid cooling rates near the electrolyte-coating interface by the surrounding

*Corresponding author: e-mail address: fcavuslu@adanabtu.edu.tr

electrolyte. However, relatively low cooling rates take place near the substrate-coating interface. As a result of these processes, coatings including a porous surface layer and a high hardness inner layer well adhered to the substrate are formed [13].

In recent years, some research has been carried out on the PEO treatment of aluminum foams. Duocel^{TM} aluminum foam (manufactured by ERG Materials and Aerospace Corp.) with an average density of $0.25\,g\,cm^{-3}$ was coated in an aqueous electrolyte solution consisting of $1.5\,g\,l^{-1}$ KOH, $10\,g\,l^{-1}$ $Na_4P_2O_7$, and $10\,g\,l^{-1}$ Na_2SiO_3 with an initial current density of $15\,A\,dm^{-2}$. It was found that the PEO treated foams exhibited similar compression peaks as uncoated foams [9]. In another study, Duocel aluminum foams with relative densities of 9–10 % and replicated foam with a relative density of 38–45 % were coated in an aqueous electrolyte solution consisting of $10\,g\,l^{-1}$ Na_2SiO_3, $2\,g\,l^{-1}$ $Na_2P_2O_7$, and $1\,g\,l^{-1}$ KOH. It was observed that the yield strength of the treated replicated aluminum foams was significantly increased, while this effect was not observed at the treated Duocel aluminum foams [10]. Moreover, in a recent study, aluminum composite foams with a relative density of 35 % were coated via PEO to enhance its compressive properties at elevated temperatures [12]. In addition to mechanical and microstructural investigations, corrosion behavior of the PEO coating on the replicated aluminum foams was studied as well [14].

The objective of this paper is to study the effect of low silicate concentration on the mechanical properties of PEO treated open-cell aluminum foams at different treatment times and current densities. Although some research has been carried out on aluminum foams treated in the higher silicate concentrations, it was reported that the average hardness of the coatings formed on the bulk aluminum alloy in silicate-rich electrolyte solution was less than that of the coatings in low silicate electrolyte [15]. The mechanical properties of the coating are affected negatively because PEO treatment in a concentrated silicate solution causes the formation of mullite phase with excessive crack and porosity. Therefore, an electrolyte solution with a low silicate concentration was employed to improve the mechanical properties of the foams after the PEO treatment.

2. Experimental procedure

In this study, porous open-celled aluminum foams with pore densities of 20 PPI and 40 PPI (pores per inch), and relative densities of 10–12 % were used. The porous aluminum foams (Trademark as Duocel) were manufactured by ERG Materials and Aerospace Corp., based in Oakland, CA, USA and were supplied in dimensions of $100 \times 100 \times 10\,mm^3$ sizes. The foams are composed of 6101-T6 aluminum alloy and are comprised of a continuous three-dimensional network of solid struts connected to each other. The average pore size was measured from SEM images as 1.037 mm and 0.864 mm for 20 PPI and 40 PPI, respectively. Aluminum foams were cut into prismoidal pieces of $20 \times 20 \times 10\,mm^3$ sizes and were coated by plasma electrolytic oxidation (PEO) treatment.

Table 1. Plasma electrolytic oxidation (PEO) treatment parameters used in this work

Time (min)	Current density ($A\,cm^{-2}$)	
	20 PPI	40 PPI
30	0.1	0.08
60	0.1	0.08
90	0.09	0.06

The PEO treatments of aluminum foams were carried out in an aqueous electrolyte solution containing $4\,g\,l^{-1}$ Na_2SiO_3, $2\,g\,l^{-1}$ $Na_2P_2O_7$, and $2\,g\,l^{-1}$ KOH. The capacitance of the system was set at 100 μF to keep the electrolyte temperature below 40 ℃. The current densities are given in Table 1 for different treatment durations.

The surface morphology and cross-section of PEO treated samples were characterized by scanning electron microscope (SEM; Philips XL300 SFEG), in secondary electron mode. The coating phases formed after the PEO treatments were investigated by X-ray diffractometer (XRD; Rigaku MiniFlex600) operated at 40 kV and 15 mA with Cu-Kα radiation (λ = 1.54 Å) between $2\theta = 20°$–$90°$, 0.02° step size, and $2°\,min^{-1}$ scan speed. XRD analysis was performed on powder samples by grinding the ceramic-coated aluminum foams with a mortar.

The uniaxial compression tests (Shimadzu AGS-X, with a 10 kN load cell) were performed over the $20 \times 20 \times 10\,mm^3$ prismoidal Duocel samples treated and untreated at a speed of $0.5\,mm\,min^{-1}$. The tests were carried out at least twice for all treatment conditions. The peak stress on the stress-strain curves was taken as the compressive strength. The yield strength was measured by drawing a line parallel to the linear region of the curve from 0.2 % plastic strain intersecting with the original curve. The energy absorption of the PEO treated and untreated foams were calculated by the integrating the stress-strain curves up to a strain of 0.3.

3. Results and discussion

3.1. Microstructure characterization

Figure 1 shows SEM images of the network

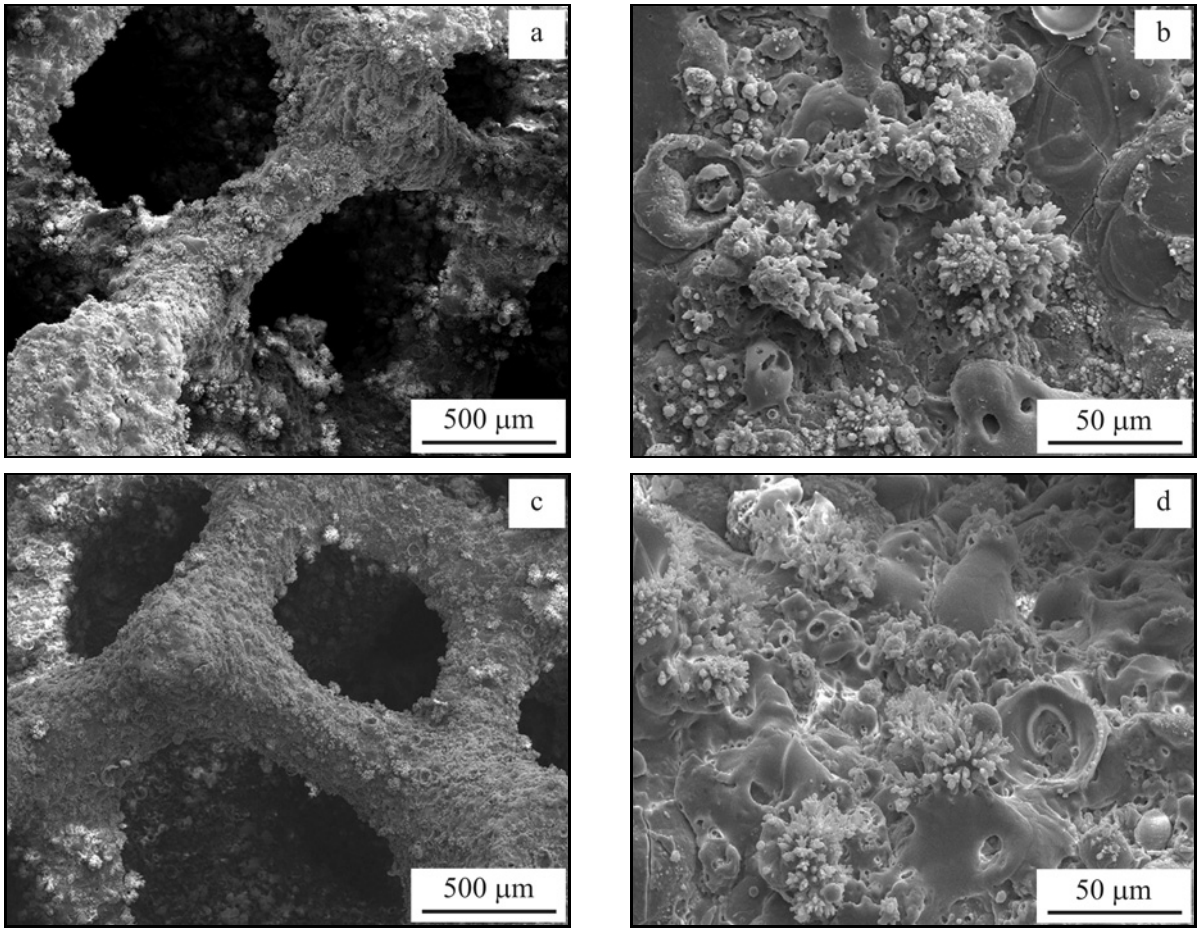

Fig. 1. SEM images of the coated aluminum foam struts treated for 90 min: (a) network structure and (b) surface morphology of the 20 PPI pore density, and (c) network structure, and (d) surface morphology of the 40 PPI pore density.

structure and surface morphology of the coated struts treated for 90 min at the current densities of $0.09\,A\,cm^{-2}$ for the pore density of 20 PPI and $0.06\,A\,cm^{-2}$ for the pore density of 40 PPI aluminum foams. The typical structural elements of PEO treatment are shown as distributed discharge channels/craters, nodular structures, and cracks. These structural elements were also obtained for all treatment conditions. The difference between the structural elements is the size of the structures that increases with increasing applied current density and treatment time. The nodular structures are the crystalline ceramic oxides, and the flower-like structures may be the amorphous silica that was not identified by the XRD pattern, but the background noise confirms the presence of an amorphous phase. The discharge channels are surrounded by molten oxides ejected through channels and rapidly solidified by contacting with electrolyte [16]. The porous nature of the surface morphology is formed as a result of these discharge channels contributing significant function in the PEO mechanism [17].

The cross-sectional SEM images of the coated aluminum foams are shown in Fig. 2. Figures 2a–c show the coated foams with the 20 PPI pore density and Figs. 2d–f show the coated foams with the 40 PPI pore density treated for 30, 60, and 90 min, respectively. The PEO treatment produced a thin coating layer for a short treatment time (30 min) and a coating consisting of two clearly distinguishable layers of a dense outer layer (1) with some cracks, discharge channels, and large pores and an inner layer (2) with distributed small pores for the long treatment times (60 and 90 min). It is seen that the discharge channels, observed as craters on the surface morphology, were formed across the outer layer.

Figure 3 illustrates the phase constituents of the foams with 20 PPI and 40 PPI pore densities treated for 30, 60, and 90 min. The thinner coating layer treated for short treatment time consists of predominantly γ-Al_2O_3 phase. Corundum (α-Al_2O_3) and mullite ($Al_6Si_2O_3$) phases were formed in addition to γ-Al_2O_3 phase with increasing treatment time. The dense outer layer consists of low-temperature alumina and aluminosilicate phases. The inner layer with distributed small pores mainly consists of a high-temperature alumina phase (α-alumina). The mullite phase is found only in the rough outer layer of the

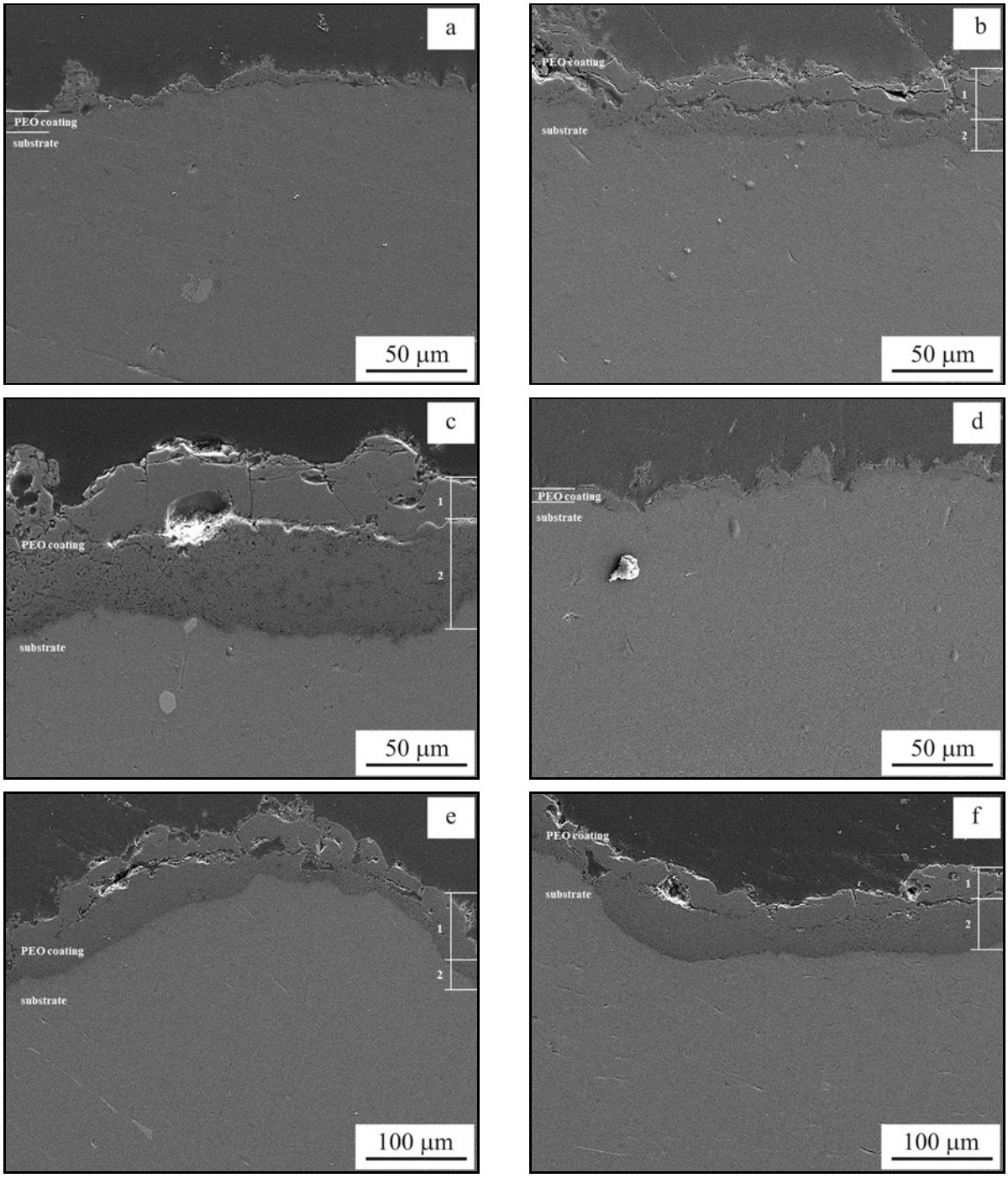

Fig. 2. Cross-sectional SEM images of the coated aluminum foams treated for (a) 30 min, (b) 60 min, and (c) 90 min with the 20 PPI pore density, (d) 30 min, (e) 60 min, and (f) 90 min with the 40 PPI pore density.

coatings for long treatment times.

The existing silicon in the form of the mullite phase comes from the electrolyte solution during the plasma electrolytic oxidation treatment. The incorporation of the silicate ions into the coating structure may be in the form of mullite or silicate phases [18]. The background noise on the XRD patterns can be the indication of the amorphous silica seen as the flower-like structure on the surface of the coating.

The average thickness of coatings treated for different times and current densities are presented in Fig. 4. The average coating thickness of the coatings for 30, 60, and 90 min treatment times is 8.36, 30.44, and 44.6 μm for 20 PPI and 10.26, 45.62, and 41.92 μm for 40 PPI pore densities, respectively. The thickness of the PEO coating increases with increasing treatment time except for the coated foam of 40 PPI for 90 min treatment time. The decrease in the coating thickness

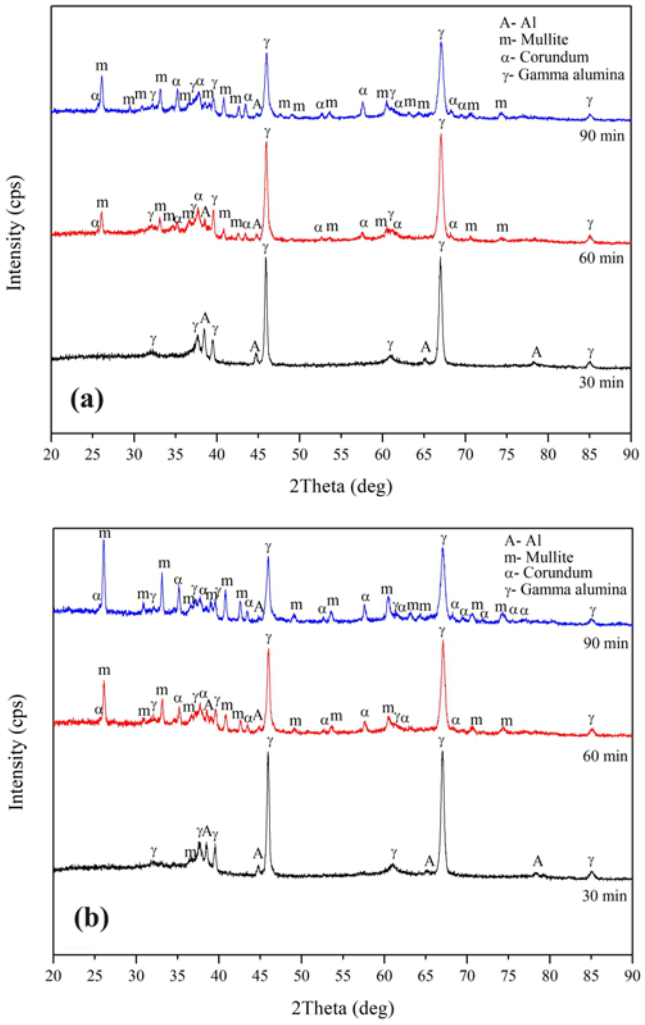

Fig. 3. XRD patterns of the PEO coated aluminum foams with the pore densities of (a) 20 PPI and (b) 40 PPI for different treatment times.

treated 90 min for 40 PPI pore density can be attributed to a couple of reasons. One is that the longer treatment time leads to a thicker coating that makes difficult for micro-arc discharges to pass through the coating. Therefore, the number of the micro-arc discharges is reduced, but they are changed into powerful discharges, and a few large arcs move across the surface releasing more energy, which may cause a destructive impact on the coating thickness as spallation [9]. Even in bulk materials during the oxidation process, the thickness of the oxidation layer could increase up to a certain thickness so as the coating growth process slows down due to the coating damage. The other reason is that the current density on the inner regions of the foam is lower than in the outer regions, which causes non-uniform current density distribution [14]. The thickness of the oxidation layer of foam materials is limited based on the width of struts. As the pore

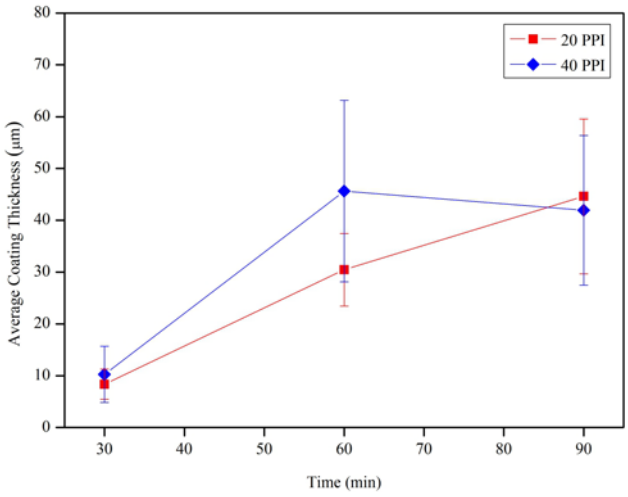

Fig. 4. The average coating thickness of the coated aluminum foams treated for different treatment times.

density of foam increases, the width of struts decreases with decreasing foam pore size [19].

3.2. Compressive properties

The compressive stress-strain curves of the samples with different pore densities are shown in Fig. 5. The density, relative density, average compressive peak stress, yield strength, specific strength, and stiffness modulus of the foams are given in Table 2. The foams exhibited typical stress-strain behavior, similar to ductile metal foam compression behavior including linear quasi-elastic, plateau, and densification regions. It can be seen that the untreated foam with 40 PPI pore density has better compressive properties than that with the 20 PPI pore density. Compared to the untreated foams, the PEO treated foams show increased strength and high elastic modulus. The increase in the compressive properties of 20 PPI pore density is greater than that of the 40 PPI pore density after the PEO treatment. The average relative density of the untreated foams is identical calculating as 11 %, and it is increased after the PEO treatment.

The compressive strength of 20 PPI pore density open-cell aluminum foams was increased after the PEO treatment. However, it was slightly improved for 40 PPI pore density aluminum foams. The slope of the quasi-elastic region of the treated foams is steeper than that of the untreated foams. The stiffness modulus of the composite foams was measured from the loading curve, and it was increased for all treatment conditions. The yield strength of the foams was improved significantly for 20 PPI pore density while it was slightly improved for 40 PPI foams. This trend was also observed for the other mechanical properties listed in Table 2. The plateau region is narrow, and the plateau stress is higher for

Table 2. The measured and calculated physical and mechanical properties of untreated and PEO treated aluminum foams at different treatment times

Pore density (pores per inch)	Treatment time (min)	Average density after PEO, ρ (g cm^{-3})	Average relative density after PEO, ρ^*/ρ_s	Average compressive peak stress, σ_c (MPa)	Average yield stress, σ_y (MPa)	Average specific strength, σ_y/ρ (MPa cm^3 g^{-1})	Average stiffness modulus, E^* (MPa)
20 PPI	Untreated	0.30	0.11	2.4 ± 0.4	1.8 ± 0.1	5.8 ± 0.2	61 ± 19
	30	0.37	0.14	4.5 ± 0.6	4.0 ± 0.5	10.5 ± 1.3	185 ± 56
	60	0.35	0.13	4.0 ± 0.4	3.6 ± 0.3	10.2 ± 0.6	198 ± 16
	90	0.36	0.13	4.0 ± 0.0	3.6 ± 0.2	10.0 ± 0.5	222 ± 26
40 PPI	Untreated	0.29	0.11	3.1 ± 0.1	2.5 ± 0.1	8.7 ± 0.5	85 ± 5
	30	0.29	0.11	3.2 ± 0.2	3.0 ± 0.1	9.9 ± 0.1	125 ± 9
	60	0.33	0.12	3.3 ± 1.1	3.0 ± 0.8	9.1 ± 1.9	144 ± 25
	90	0.36	0.13	3.3 ± 0.5	2.8 ± 0.7	7.6 ± 1.6	179 ± 14

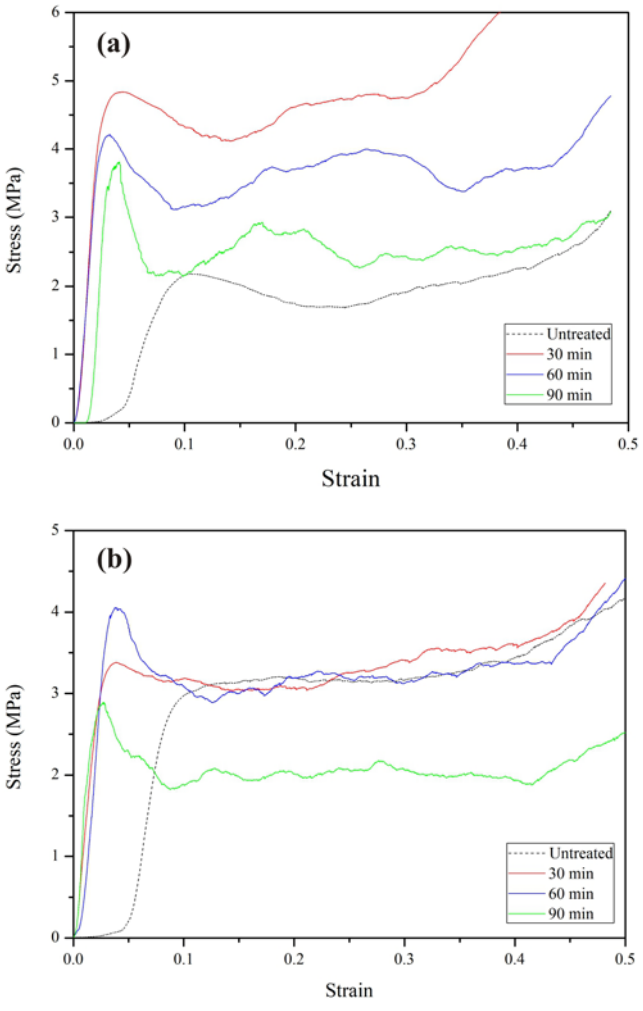

Fig. 5. The uniaxial compressive stress-strain curves of coated aluminum foams with the pore densities of (a) 20 PPI and (b) 40 PPI for different treatment times.

the 30 min treatment time with the pore density of 20 PPI.

The pore density is the main parameter that affects the materials properties. However, the relative density can also influence the mechanical properties. For the same pore density, the bending moment of the foams depends on the relative density because it influences the neutral bending axis of the struts [8]. Foams with the pore densities of 20 PPI exhibited higher mechanical properties with increasing relative density whereas the 40 PPI foams exhibited lower or same level because of the thinner struts. With the decrease in strut thickness as in the case of 40 PPI, the coating to metal ratio is critical because the foam exhibits brittle failure.

In the literature, Dunleavy et al. [9] reported that the specific strength of the PEO treated open-cell aluminum foam showed approximately the same peak stress with the untreated foam. In another study, Abdulla et al. [10] found that the specific strength of the aluminum foam was 9.2 MPa cm^3 g^{-1}, which was the highest specific strength obtained in their work. In this study, the highest average specific strength is 10.46 MPa cm^3 g^{-1}, corresponding to 80 % increase for 20 PPI foam treated for 30 min.

Figure 6 shows the energy absorption of the foams calculated by integrating the stress-strain curves up to a strain of 0.3 for untreated and treated composite foams. It is seen that PEO treated 20 PPI foams absorbed more energy than PEO treated 40 PPI foams. The energy absorbed per unit volume of foams is decreased with increasing treatment time. Since the pore sizes of the 40 PPI and 20 PPI foams are 0.864 and 1.037 mm, the strut thickness of 40 PPI foams is lower than that of 20 PPI foams. Thus, the conversion fraction of aluminum struts to ceramic coating is greater for 40 PPI pore density, and the coating is almost entirely buckled down as soon as the onset of the yielding starts followed by the bending of the metal struts at nearly constant plateau stress. It is well known that ceramics fail in a brittle manner, unlike metals that fail in a plastic manner. This is due to the formation

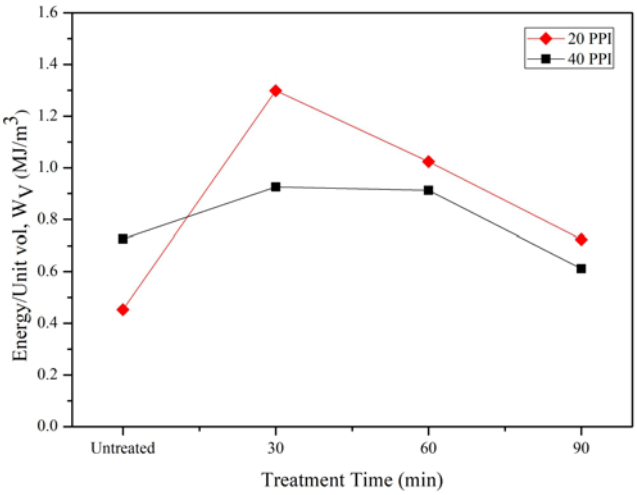

Fig. 6. Energy absorption of untreated and PEO treated aluminum foams for different treatment times.

of microcracks and pores at the surface of the coating. Thermal stresses caused by the discharge phenomena during the coating process lead to the formation of cracks. PEO coatings of the longer treatment times (60 and 90 min) prominently have such defects distributed across the surface that affect the mechanical properties negatively. The increase in the specific strength of the coating with longer treatment times is less than the one with the shorter treatment time (30 min) due to the mullite phase and defects formation.

4. Conclusions

In the present study, open-cell aluminum foams, trademark as Duocel with the pore densities of 20 PPI and 40 PPI were coated by plasma electrolytic oxidation treatment at different treatment parameters. Microstructure and XRD investigations revealed that PEO coatings are composed of a dense thin surface layer consisting of mainly γ-Al_2O_3 phase for a short treatment time, while coatings are composed of a dense surface layer with discharge channels, some cracks and large pores and an inner layer with distributed small pores consisting of corundum (α-Al_2O_3) and mullite ($Al_6Si_2O_3$) phases besides γ-Al_2O_3 phase for long treatment times. The compression test results showed that the mechanical properties of the composite foams with the pore density of 20 PPI treated for 30 min was sufficiently improved, compared to 60 and 90 min. However, the mechanical properties of the composite foams with the pore density of 40 PPI were not improved, as much as the pore density of 20 PPI.

Acknowledgements

This study was supported by Gebze Technical University Scientific Research Projects Office (project No. 2015--A-35). The authors would like to thank the Scientific and Technological Research Council of Turkey (TÜBİTAK) for funding the first author within TÜBİTAK-BİDEB 2211-C National Doctorate Scholarship Program.

References

[1] Gibson, L. J., Ashby, M. F.: Cellular Solids: Structure and Properties. Cambridge, Cambridge University Press 1997. doi:10.1017/CBO9781139878326
[2] Banhart, J.: Progress in Materials Science, *46*, 2001, p. 559. doi:10.1016/S0079-6425(00)00002-5
[3] Ashby, M. F., Evans, A. G., Fleck, N. A., Gibson, L. J., Hutchinson, J. W., Wadley, H. N. G.: Metal Foams: A Design Guide. Oxford, Butterworth-Heinemann 2000.
[4] Alizadeh, M., Mirzaei-Aliabadi, M.: Materials & Design, *35*, 2012, p. 419. doi:10.1016/j.matdes.2011.09.059
[5] Boonyongmaneerat, Y., Schuh, C., Dunand, D.: Scripta Materialia, *59*, 2008, p. 336. doi:10.1016/j.scriptamat.2008.03.035
[6] Bouwhuis, B. A., McCrea, J. L., Palumbo, G., Hibbard, G. D.: Acta Materialia, *57*, 2009, p. 4046. doi:10.1016/j.actamat.2009.04.053
[7] Devivier, C., Tagliaferri, V., Trovalusci, F., Ucciardello, N.: Materials & Design, *86*, 2015, p. 272. doi:10.1016/j.matdes.2015.07.078
[8] Bele, E., Bouwhuis, B. A., Codd, C., Hibbard, G. D.: Acta Materialia, *59*, 2011, p. 6145. doi:10.1016/j.actamat.2011.06.027
[9] Dunleavy, C. S., Curran, J. A., Clyne, T. W.: Composites Science and Technology, *71*, 2011, p. 908. doi:10.1016/j.compscitech.2011.02.007
[10] Abdulla, T., Yerokhin, A., Goodall, R.: Materials & Design, *32*, 2011, p. 3742. doi:10.1016/j.matdes.2011.03.053
[11] Abdulla, T., Yerokhin, A., Goodall, R.: Scripta Materialia, *75*, 2014, p. 38. doi:10.1016/j.scriptamat.2013.11.012
[12] Liu, H., Pan, W., Si, F., Huang, K. F., Liu, Y., Liu, J.: Metals, *8*, 2018, p. 118. doi:10.3390/met8020118
[13] Yerokhin, A. L., Nie, X., Leyland, A., Matthews, A., Dowey, S. J.: Surface and Coatings Technology, *122*, 1999, p. 73. doi:10.1016/S0257-8972(99)00441-7
[14] Liu, J., Zhu, X., Huang, Z., Yu, S., Yang, X.: Journal of Coatings Technology and Research, *9*, 2011, p. 357. doi:10.1007/s11998-011-9377-3
[15] Kalkanci, H., Kurnaz, S. C.: Surface and Coatings Technology, *203*, 2008, p. 15. doi:10.1016/j.surfcoat.2008.07.015
[16] Sundararajan, G., Rama Krishna, L.: Surface and Coatings Technology, *167*, 2003, p. 269. doi:10.1016/S0257-8972(02)00918-0
[17] Polat, A., Makaraci, M., Usta, M.: Journal of Alloys and Compounds, *504*, 2010, p. 519. doi:10.1016/j.jallcom.2010.06.008
[18] Xin, S. G., Song, L. X., Zhao, R. G., Hu, X. F.: Materials Chemistry and Physics, *97*, 2006, p. 132. doi:10.1016/j.matchemphys.2005.07.073
[19] Korkmaz, K.: Surface and Coatings Technology, *272*, 2015, p. 72. doi:10.1016/j.surfcoat.2015.04.022